Research Square

Preprints are preliminary reports that have not undergone peer review.
They should not be considered conclusive, used to inform clinical practice,
or referenced by the media as validated information.

Chronic exposure to interleukin-10 drives inflammaging and accelerated tissue senescence

Margarida Saraiva

margarida.saraiva@i3s.up.pt

i3S - University of Porto https://orcid.org/0000-0002-8180-1293

Ana Martins

i3S - University of Porto

Rita Santos

i3S - University of Porto

Inês Faria

i3S - University of Porto

José Pedro Castro

Universidade do Porto https://orcid.org/0000-0002-2627-5331

Rute Gonçalves

i3S - University of Porto

Carlos Sousa-Soares

i3S - Instituto de Investigação e Inovação em Saúde, Universidade do Porto

Marcos Cardoso

i3S - University of Porto

Tania Lima

i3S - University of Porto

Elsa Silva

i3S

Rita Gomes

INEB – Instituto Nacional de Engenharia Biomédica, i3S – Instituto de Investigação e Inovação em Saúde, Universidade do Porto, 4200-135 Porto,

Sofia Pacheco

i3S - University of Porto https://orcid.org/0009-0008-5527-5956

Isabel Castro

ICVS, School of Medicine, University of Minho

Irina Amorim

i3S - University of Porto

Diana Nascimento

i3S - University of Porto

Nuno Osorio

ICVS, School of Medicine, University of Minho

Antonio Castro

ICVS, School of Medicine, University of Minho

Paulo Vieira

Institut Pasteur

Elsa Logarinho

Universidade do Porto

Article

Keywords:

Posted Date: March 13th, 2026

DOI: https://doi.org/10.21203/rs.3.rs-8603195/v1

License: This work is licensed under a Creative Commons Attribution 4.0 International License. Read Full License

Additional Declarations: There is **NO** Competing Interest.

Abstract

Interleukin (IL)-10, a major anti-inflammatory cytokine, can paradoxically have pro-inflammatory activities, which limits the efficacy of IL-10-based therapies. We previously showed that in vivo exposure to therapeutic doses of IL-10 reprograms T cells and promotes interferon (IFN)-γ-mediated emergency myelopoiesis. Here, we show that chronic IL-10 elevation in mice reprograms CD4+ and CD8+ T cells to display transcriptional and functional signatures of senescence. Furthermore, these T cells infiltrate and cause structural and functional alterations in the spleen, gonadal white adipose tissue and pancreas. Lack of T cells resulted in virtually no phenotype, whereas IFN-γ was only partly involved. Importantly, interrogation of several mouse and human datasets revealed a correlation between IL-10 levels and the IL-10-induced T cell signature with physiological aging. Altogether, we report a novel mouse model of sterile inflammaging and highlight a previously unappreciated role for IL-10 in accelerating aging, which is conserved in mice and humans. Our study opens new avenues on the basic biology and clinical use of IL-10.

Introduction

Interleukin (IL)-10 is an anti-inflammatory cytokine with key roles in regulating immune responses [1]. For this reason, IL-10 has garnered substantial clinical interest as an anti-inflammatory modulating agent. However, its therapeutic success has been limited, partly due to the existence of several side-effects [2]. Indeed, administration of IL-10 to humans, although relatively well tolerated [3], led to hematologic alterations that included monocytosis, thrombocytopenia and anemia [4-6]. Furthermore, increased levels of interferon (IFN)-g were detected in the serum of volunteers receiving IL-10 [7]. We previously showed that IL-10 elevation *in vivo* unexpectedly reprogrammed bone marrow (BM) T cells to produce IFN-g, driving emergency myelopoiesis, thus providing a mechanistic basis for the reported hematologic alterations [8]. Further links between IL-10 and myelopoiesis were subsequently found: a myeloid-like IL-10-producing B cell subset was identified in the mouse BM upon LPS injection and shown to boost emergency myelopoiesis in an IL-10-dependent manner [9]; in lethal hyperinflammatory disease promoted by excessive IL-10 and IL-18 in mice, an IL-10-driven shift of hematopoiesis towards enhanced myelopoiesis was observed [10]. In contrast, maternal IL-10 was reported to restrict fetal hematopoietic stem and progenitor cells from activating emergency myelopoiesis [11]. Collectively, these studies highlight a dose and context dependent role for IL-10 as a regulator of hematopoiesis.

Although IL-10 is classically known to act on myeloid cells to control T cell responses [1], several studies have shown that IL-10 can reprogram T cells *in vivo* towards an activated phenotype. Our previous study demonstrated that *in vivo* IL-10 elevation induced the contraction of the BM naïve $CD4^+$ and $CD8^+$ T cell compartments and enhanced the expression of PD1 and CD38, and the production of IFN-g by these cells [8]. IL-10 exerts anti-tumour activity by inducing the expansion and activation of $CD8^+$ T cells that express IFN-g and GzmB [12-15]. Also, T-cell-derived IL-10 was shown to enhance inflammation in experimental autoimmune encephalomyelitis by acting on effector T cells and promoting their survival [16]. In a model of

chronic lymphocytic leukemia (CLL), IL-10 signaling was found to control the balance between exhausted and functional $CD8^+$ T cells, impairing CLL progression [17]. Thus, the pro-inflammatory properties of IL-10 through the reprogramming of T cells are likely crucial to the success or failure of IL-10-based therapies, calling for a better understanding of the full biological properties of this cytokine in the organism.

Interestingly, some of the features found in IL-10-reprogrammed T cells, namely the contraction of the naïve compartment, the overall pro-inflammatory phenotype characterized by the expression of exhaustion and cytotoxicity markers, and IFN-g production, are shared with T cell subsets that emerge in aged individuals [8,18-20]. Indeed, T cells are among the immune cell populations that change more in aging, upregulating the expression of exhaustion and cytotoxic markers, and displaying enhanced migration to nonlymphoid tissues where they contribute to cellular senescence and inflammaging, ultimately leading to tissue deterioration [20-22]. Intriguingly, previous studies have reported an increase of seric IL-10 with age in both humans and mice [23,24]. In contrast, however, polymorphisms in the *IL10* promoter leading to higher IL-10 expression are more prevalent in Caucasian centenarians than in younger subjects [25] and lower levels of IL-10 in elderly men correlated with higher risk of frailty-associated pathologies [26]. Signs of accelerated frailty are also described in *Il10* deficient mice, likely as a consequence of the persisting low grade pro-inflammatory state seen in this model [27,28]. Therefore, the role of IL-10 in aging remains controversial and whether the IL-10-mediated inflammation seen upon elevation of IL-10 *in vivo* contributes to accelerated aging remains largely unknown.

In this study, we sought to investigate if IL-10-reprogrammed T cells generated *in vivo* display molecular features of accelerated aging and, most importantly, whether they contribute to systemic tissue damage, in addition to emergency myelopoiesis and hematologic alterations. We found that both $CD4^+$ and $CD8^+$ T cells exposed to IL-10 *in vivo* display transcriptional and functional molecular signatures of senescence, migrate to non-lymphoid organs, and cause structural and functional alterations in adipose tissue and pancreas. Analysis of mouse and human RNA and protein datasets of physiological aging revealed a conserved phenotype, characterized by the accumulation of IL-10 transcripts and protein and by the expression of an IL-10-dependent T cell transcriptional signature in aged individuals. Besides their impact on the design of IL-10-based therapies, our findings implicate IL-10 as a novel player in aging and uncover *in vivo* IL-10 elevation as an unique inflammation-based model of accelerated aging.

Results

Elevation of IL-10 levels *in vivo* induces T cell senescence in the bone marrow and spleen

We have previously investigated the alterations induced *in vivo* by IL-10 elevation using the pMT-10 mouse model [29]. We showed that IL-10 doses approaching those used in therapeutic settings reprogram the BM CD4 and CD8 T cell compartment [8]. In line with our previous study, elevation of IL-10 for 30 days in pMT-10 mice resulted in a contraction of the BM naïve ($CD44^-CD62L^+$) T cell pool and the accumulation of highly activated $PD\text{-}1^+CD38^+$ $CD4^+$ and $CD8^+$ T cells (Figure 1a, b; Supp Figure 1a-c). These alterations to the T cell pool were not observed in zinc-induced C57BL/6, neither in non-induced pMT-10 nor in induced pMT-

10.IL10Ra$^{-/-}$ control mice (Figure 1a, b; Supp Figure 1a-c). Furthermore, and despite the absence of major alterations to the total numbers of BM CD3^{+} cells (Supp Figure 1d), induced pMT-10 mice showed an increased ratio of CD4/CD8 T cells as compared to all control groups (Supp Figure 1e).

Since the changes described above in the T cell compartment are reminiscent of T cell aging [30], we next examined if exposure to high doses of IL-10 *in vivo* might trigger molecular features of senescence in T cells, namely high SA-β-galactosidase activity and DNA damage [31-33]. Flow cytometry analyses of BM T cells (Supp Figure 1a) showed an increase of both SA-β-gal^{+} and phosphorylated H2A histone family member X (γH2AX)$^{+}$ CD4^{+} (Figure 1c) and CD8^{+} (Figure 1d) T cells in induced pMT-10. We also investigated whether the transcriptome of IL-10-reprogrammed T cells displayed signatures of aging/senescence. Based on previous studies [18,19], we curated a transcriptomic signature of aged/senescent T cells (see Methods section), including genes encoding senescence-associated secretory phenotype (SASP) proteins, or molecules linked to T cell exhaustion/senescence phenotypes. This transcriptomic signature was then used to interrogate our previously generated RNA-seq datasets of BM CD4^{+} and CD8^{+} T cells exposed to IL-10 *in vivo* [8]. When compared to C57BL/6 or pMT-10 control groups, BM CD4^{+} and CD8^{+} T cells of induced pMT-10 mice were indeed enriched for the transcriptional signature of senescence (Figure 1e; Supp Table 1 and 2). Furthermore, this signature was downregulated in CD4^{+} and CD8^{+} T cells from induced pMT-10 lacking the IL-10Ra chain, showing that its expression depends on IL-10 signaling (Figure 1f; Supp Table 1 and 2). The global transcriptional directionality imposed by IL-10 was similar and highly significant in CD4^{+} and CD8^{+} T cells (Supp Figure 1f), suggesting that common mechanisms of IL-10-reprogramming occur in these T cell subsets.

The accumulation of senescent T cells in circulation has been described in aging [32]. In induced pMT-10 mice an accumulation of PD-1^{+}CD38^{+} T cells in the BM was observed between days 5 and 10 post-Zinc administration, which remained evident on day 30 post-IL-10 induction (Supp Figure 1g). A marked increase of this population was visible also in the blood, but only after 30 days of IL-10-induction (Supp Figure 1h). This led us to question whether IL-10 elevation would be sufficient to accelerate the biological age of induced mice based on established blood DNA methylation clocks (DNAmAge). Indeed, we found increased scores, although not-statistically significant, of the DNAmAgePan or DNAmAgePanInterventions clocks [34,35] in induced pMT-10 mice (Supp Figure 1i, j), suggesting that IL-10/IL-10-reprogrammed T cells may be contributing to accelerated (epigenetic) aging in the blood pool.

Further supporting the notion that the IL-10-reprogrammed T cells are not restricted to the BM, induced pMT-10 mice displayed decreased CD44^{-}CD62L^{+} naïve and increased PD-1^{+}CD38^{+} frequencies among splenic CD4^{+} and CD8^{+} T cells (Supp Figure 2a, b), as well as an accumulation of T cells displaying senescence markers (Supp Figure 2c, d). The differences observed in the BM (Figure 1a-d) were, however, globally more pronounced than those detected in the spleen. Because aged T cells often display mitochondrial abnormalities [21], we investigated the mitochondrial status of splenic CD4^{+} and CD8^{+} T cells from induced pMT-10 mice, combining TEM and flow cytometry. Analyses and quantification of TEM images showed that the number of preserved mitochondria per cell was similar in control or pMT-10-

induced mice (Supp Figure 2e, f, g, i). This result was further validated by flow cytometry, as we did not detect an accumulation of damaged mitochondria (MitoTracker Green^{high}/MitoTracker Red^{low}) in response to IL-10 elevation (Supp Figure 2h, j). However, a statistically significant reduction in functional mitochondria (MitoTracker Green^{high}/MitoTracker Red^{high}) was observed in both T cell populations (Supp Figure 2h, j).

Taken together, our data indicate that exposure of T cells to elevated levels of IL-10 *in vivo* triggers an earlier accumulation of cells with senescence phenotypes in the BM (day 10), which can also be detected in the blood and spleen on day 30 post-IL-10 induction.

High levels of IL-10 induce structural and functional alterations in non-lymphoid organs

Senescent T cells have been described to contribute to organismal aging by infiltrating different non-lymphoid tissues and promoting their decline [21,22]. Thus, we next performed histological analyses of several tissues in C57BL/6 control or induced pMT-10 mice. Cellular infiltrates were detected in gWAT, colon, pancreas and lungs of induced pMT-10 mice (Figure 2a; Supp Figure 3a). Striking histologic alterations were observed in these mice in gWAT, with the presence of “crown-like” structures [36] surrounding the adipocytes (Figure 2a), and in the pancreas, which displayed a profoundly altered structure (Figure 2a). IL-10 induction did not result in evident cellular infiltrates or histologic alterations in the heart or liver (Figure 2a; Supp Figure 3a). Given the presence of cellular infiltrates in gWAT, colon, pancreas and lung of induced mice, we further analysed these tissues by flow cytometry. We found a significant increase in the frequency of PD-1^{+}CD38^{+} T cells after IL-10 induction (Figure 2b), accompanied by an increase in the frequency of T cells in the case of gWAT and colon (Figure 2b). Flow cytometry analysis of the hearts of IL-10-induced mice also revealed increased frequencies of T cells and PD1^{+}CD38^{+} T cells (Supp Figure 3b). Therefore, we cannot exclude a wider infiltration of PD1^{+}CD38^{+} T cells in organs upon IL-10 induction.

Because the most prominent alterations were detected in the gWAT and pancreas, we analysed these tissues in more detail. Crown-like structures are a sign of adipose tissue inflammation and are normally associated with cellular senescence processes [36]. In line with this, a markedly increased frequency in SA-β-gal activity was found in gWAT from induced pMT-10 mice (Figure 2c). Furthermore, the average adipocyte area was decreased in IL-10 exposed animals (Figure 2d), a feature previously associated with increased age [37]. Of note, accompanying these alterations of adipose tissue, induced pMT-10 mice displayed lower body weight than control C57BL/6 from 2 weeks post-IL-10 induction (Supp Figure 3c). The histological score of the pancreas [38] revealed tissue pathology (Figure 2e), accompanied by a significant decrease of amylase and lipase levels in the serum (Figure 2f) in IL-10-induced mice. These findings indicate damage to the pancreas, with signs of pancreatitis, paralleling that reported in aged mice [22]. Despite the presence of PD1^{+}CD38^{+} T cell infiltrates in the colon, lungs and heart of induced pMT-10 mice (Figure 2b and Supp Figure 3b), we did not observe alterations to the colon length (Supp Figure 3d), evidence of lung edema (Supp Figure 3e), nor alterations to the cardiomyocyte area or the ratio heart weight/body weight (Supp Figure 3f) in induced mice, 30 days post-induction. Of note, increased alanine aminotransferase/glutamic pyruvic transaminase (ALT/GPT) ratio and decreased albumin levels, but no alteration on aspartate

aminotransferase/ glutamic-oxaloacetic transaminase (AST/GOT) ratio or total bilirubin levels were detected in the serum of induced pMT-10 mice (Supp Figure 3g), possibly indicating inflammation in the absence of overt liver damage. Finally, no biochemical alterations linked to kidney mal-function were detected in the serum of induced pMT-10 animals on day 30 post-induction (Supp Figure 3h). Altogether, these data indicate that the IL-10 reprogrammed T cells infiltrate non-lymphoid tissues, with gWAT and pancreas undergoing a prominent series of structural and functional alterations as early as day 30 post-IL-10 induction, suggestive of accelerated aging.

IL-10-induced alterations to the adipose tissue and pancreas are T cell-dependent

Since we previously showed that emergency myelopoiesis caused by IL-10 elevation occurred in a IFN-γ- and T cell-dependent manner [8], we next investigated whether IFN-γ and T cells were also required for senescence and tissue damage. We investigated the requirement for IFN-γ in the T cell reprogramming, by analysing the BM T cell pool of induced pMT-10.IFN-$\gamma^{-/-}$ mice. In the absence of IFN-γ, IL-10 induced mice showed an overall contraction of the BM $CD4^+$ and $CD8^+$ naive T cell pools, along with increased frequency of PD-1^+ and $CD38^+$ T cells (Figure 3a). Interestingly, the baseline (non-induced) levels of SA-βgal^+ BM T cells were higher in pMT-10.IFN-$\gamma^{-/-}$ mice (5,57%±0,2717 $CD4^+$ and 4,76%±0,8067 $CD8^+$) than in pMT-10.IFN-$\gamma^{+/+}$ mice (1,39%±0,1638 $CD4^+$ and 0,54%±0,09579 $CD8^+$) (compare Supp Figure 4a with Figure 1c, d above) and induction of IL-10 did not increase the frequency of SA-βgal^+ T cells in the BM of pMT-10.IFN-$\gamma^{-/-}$ mice (Supp Figure 4a). However, the frequency of $\gamma H2AX^+$ $CD4^+$ and $CD8^+$ T cells was significantly increased in induced pMT-10.IFN-$\gamma^{-/-}$ animals (Supp Figure 4a). Transcriptomic analysis of BM $CD4^+$ and $CD8^+$ T cells purified from induced pMT-10.IFN-$\gamma^{-/-}$ mice showed that the absence of IFN-γ did not significantly impact the T cell signature of SASP, exhaustion and senescence (Figure 3b; Supp Tables 3 and 4). Based on these data, we fine-tuned an IL-10-induced transcriptional signature (see methods) and performed GSEA of this signature in the transcriptome of $CD4^+$ and $CD8^+$ T cells purified from pMT-10 or pMT-10.IFN-$\gamma^{-/-}$ mice induced or not with zinc. As expected, the GSEA analyses confirmed no impact of IFN-γdeficiency in the IL-10-driven transcriptional signature (Supp Figure 4b). When analyzing hallmark pathways by GSEA, we found that IL-10 overexpressing IFN-γ-competent or deficient mice are very similar, in both $CD4^+$ and $CD8^+$ T cells (Supp Figure 4c). Notably, many of the upregulated pathways overlap with aging-associated signatures observed across species [39]. Among these are pathways related to inflammatory processes (e.g. TNF signaling via Nfkb, IL-2-STAT5 signaling, complement), apoptosis, stress (e.g. MTORC1 signaling, glycolysis) and cell cycle (e.g. E2F targets, G2M checkpoint). Of note, the “interferon-gamma response” pathway was still detected in induced pMT-10.IFN-$\gamma^{-/-}$ mice, albeit to a lesser degree than in induced pMT-10 mice (Supp Figure 4c). Thus, IFN-γ is not required for reprogramming of BM $CD4^+$ and $CD8^+$ T cells driven *in vivo* by IL-10 induction.

Next, we examined the contribution of IFN-γ and T cells to the phenotypic alterations induced by IL-10 elevation in the gWAT and pancreas. Analysis of the gWAT of induced pMT-10.IFN-$\gamma^{-/-}$ mice revealed a significant accumulation of $PD1^+CD38^+$ T cells, although less marked than that observed in induced IFN-γ competent mice (Supp Figure 4d). In parallel, gWAT and pancreas of induced pMT-10.IFN-$\gamma^{-/-}$ and pMT-

10.CD3$^{-/-}$ mice were harvested for histologic analysis. The presence of cellular infiltrates was detected in the gWAT of some but not all induced pMT-10.IFN-γ$^{-/-}$ mice (Figure 3c; Supp Figure 4e). Furthermore, the average adipocyte area of induced pMT-10.IFN-γ$^{-/-}$ was statistically not different from that of non-induced control mice (Figure 3d), and above the average values previously observed for pMT-10.IFN-γ$^{+/+}$ mice (see Figure 2d). Although some pMT-10.IFN-γ$^{-/-}$ mice still showed SA-β-gal activity in their gWAT (Figure 3e), the penetrance of this phenotype was markedly reduced compared to IFN-γ competent mice (see Figure 2c). In contrast to the partial effect observed in the absence of IFN-γ, lack of CD3^{+} T cells almost completely abrogated the IL-10-induced gWAT phenotype across these parameters (Figure 3c-e). Similarly to gWAT, we observed a less prominent IL-10-induced phenotype in the pancreas of pMT-10.IFN-γ$^{-/-}$ mice, with most of the animals showing pancreatic infiltrates (Supp Figure 4e). The pancreatic histologic score was increased in induced pMT-10.IFN-γ$^{-/-}$ mice (Figure 3f, g), but not as pronounced as in IFN-γ competent mice. In addition, the levels of amylase and lipase found in the serum of both control and induced pMT-10.IFN-γ$^{-/-}$ mice were not altered (Figure 3h). Absence of CD3^{+} T cells fully protected the pancreas from the damage caused by IL-10 elevation (Figure 3f-h).

Altogether, these data indicate that the IL-10-induced phenotype in the gWAT and pancreas is T cell-dependent, similarly to IL-10-driven emergency myelopoiesis [8]. IFN-γ, a cytokine that mediates IL-10-dependent emergency myelopoiesis, is not required for the IL-10-dependent reprogramming of T cells, and only partially accounts for the aging phenotypes induced by T cell paracrine signaling in non-lymphoid organs.

Dynamics of IL-10 in mouse aging

To ascertain for a role of IL-10 in T-cell mediated physiological aging, we next used the T cell signature derived from IL-10 induction to interrogate previously published scRNAseq datasets obtained from murine tissues at 3, 18 and 24 months of the life span [40]. We started by analysing the BM, the lymphoid organ where the IL-10-induced phenotype starts, and the gWAT, a non-lymphoid organ highly affected by IL-10 induction. In both organs, several cell clusters were identified, including immune and non-immune cells (Figure 4a). The IL-10 transcriptional signature was detected as early as 3 months of age, particularly in lymphoid populations, its intensity score increased at 18 months and peaked at 24 months (Figure 4a). At this stage, in the BM the *Il10* signature was mainly detected in T cells, but in the gWAT it was also detected in myeloid cells (Figure 4a). Expanding these analyses to the spleen and the pancreas showed very similar observations (Supp Figure 5a).

Next, we interrogated the *Tabula Muris Senis* dataset [41] to investigate how the *Il10* transcriptional signature correlated with the mouse age and/or with the expression of *Il10* during the mouse lifespan. A positive correlation of the *Il10* transcriptional signature with aging (Figure 4b) and with the expression of *Il10* during aging (Figure 4c) was detected in the BM, spleen and gWAT, but not in the pancreas. Positive correlations between the *Il10* transcriptional signature and aging (Supp Figure 5b) and with the expression of *Il10* as the age of the mouse increased (Supp Figure 5c) were also generally detected for the other tested organs.

We then hypothesized that differences in correlations detected across distinct organs might depend on organ-specific expression patterns of *Il10*, *Il10ra* and *Il10rb* along the mouse lifespan. By further interrogating the *Tabula Muris Senis* dataset, we found that the expression of *Il10* was positively correlated with agein the BM, spleen and gWAT, although not in the pancreas (Figure 4d). Interestingly, in the gWAT a strong correlation was also detected between the expression of both chains of the *Il10r* and aging (Figure 4d), possibly contributing to the overt phenotype observed in this tissue after IL-10 induction. Expanding the analysis to other organs, which were either not affected or not analysed in our model, identified tissues displaying a positive or negative correlation between the expression of *Il10* or its receptors and aging (Supp Figure 5d).

Finally, we performed GSEA for the IL-10-transcriptional signature against 5 available signatures [39,42]: two from normal aging (multi-tissue and liver), one from a reprogramming intervention (liver) and two from lifespan extending interventions associated to maximum lifespan and median lifespan (see methods). A positive NES was obtained for the *Il10* signature in both aging signatures, whereas a negative NES was detected for the rejuvenating interventions (Figure 4e).

Collectively, these results highlight the enrichment of the IL-10-driven T cell signature during normal aging and its repression in the context of lifespan extending interventions. They also suggest that during aging, the dynamics of *Il10* and IL-10-transcriptional signature mounts at a different pace in distinct tissues.

Dynamics of IL-10 in human aging

Elevated serum IL-10, together with signs of immunosenescence, was reported in a subset of patients with common variable immunodeficiency (CVID) [43] and in patients with severe COVID-19 [44]. High levels of circulating IL-10 were also reported in aged humans [24]. We therefore went on to investigate whether the results found in mouse aging were also found in humans. We interrogated a previously analysed plasma proteome database from over 50,000 human subjects in the UK Biobank [45] for proteins encoded by the human homologues of the 21 transcripts comprising the mouse-derived T cell IL-10-signature. We found a significant positive correlation between plasma levels of twelve of these proteins, including IL-10, and chronological age (Figure 5a). We thus asked if a transcriptional signature homologous to the mouse IL-10-induced signature was also observed in human immune cells with aging. We analyzed scRNA-seq data obtained for several immune cell types from donors of two distinct age cohorts (over 40-years-old versus under 40-years-old) [46]. This dataset allowed us to evaluate transcriptional changes in immune cells from the blood, bone marrow and spleen, tissues that were affected by IL-10 elevation in the pMT-10 mouse model. GSEA analysis showed that the transcriptional signature induced by IL-10 was upregulated in these tissues, in older humans, across multiple cell types (Figure 5b). These included several T cell, NK cell, B cell, and myeloid cell populations (Figure 5b). Among the T cell populations in these organs, upregulation of the IL-10 transcriptional signature was most evident in terminal effector subsets such as $CD4^+$ TEMRA, $CD8^+$ TEMRA, $CD4^+$ TEM and $CD8^+$ TEM (Figure 5c and Supp Figure 6). In central memory T cells and regulatory T cells, which showed relatively low expression of the IL-10 signature already in young donors, this signature was decreased with age (Figure 5b, c and Supp Figure 6). Thus, in the human system, a positive correlation between IL-10 and the IL-10 signature expression levels and age exists, as we found in mice.

Discussion

Chronic low-grade inflammation is a central mediator of organismal aging (known as inflammaging) and several cytokines play key roles in this process [47]. TNF neutralization reversed accelerated aging in a model of T cell dysfunctional mitochondria [21] and inhibition of IL-11 was recently demonstrated to extend mammalian health and lifespan [48]. Despite its classical anti-inflammatory properties, an increase of circulating IL-10 has been also described in aged mice and humans [23,24]. Here we show that, unexpectedly, IL-10 may also drive accelerated aging when administrated at levels currently explored in the clinic against conditions such as inflammatory bowel disease, rheumatoid arthritis and cancer [3,6,7,14,15].

As reported in our previous study [8], *in vivo* elevation of IL-10 changed the composition of both $CD4^+$ and $CD8^+$ BM T cell compartments, leading to a marked contraction of naïve T cells and accumulation of $CD4^+$ and $CD8^+$ T cells expressing high levels of PD1 and CD38. We now show that, additionally, IL-10 elevation imposes transcriptional and functional alterations that are common to both $CD4^+$ and $CD8^+$ T cells and that parallel the phenotypes reported in T cells of aged humans and mice, where a reorganized $CD4^+$ T cell compartment [18,49,50] and terminally differentiated $CD8^+$ T cells with senescent characteristics [19] were described. We show that the IL-10-mediated alterations to the T cell phenotype start in the BM, where an increase of $PD1^+CD38^+$ T cells is noticeable as early as 10 days post-IL-10 induction. By day 30 we detect these cells in the blood and the spleen of pMT-10 mice. Aged T cells are known to display altered homing patterns, characterized by a shift from lymphoid to non-lymphoid preference, and to inflict tissue damage where they infiltrate [20]. Accordingly, we also found increased frequencies of IL-10-reprogrammed $PD1^+CD38^+$ T cells in several non-lymphoid tissues. In the time-frame investigated here, i.e. 30 days of exposure to elevated IL-10, the main tissue architecture and functional alterations detected were to the gWAT and the pancreas. The relatively fast effect of IL-10 elevation on the gWAT is likely related to the vulnerability of this tissue to aging [36]. Indeed, in normal aging widespread activation of immune cells is first detectable in WAT depots [51] and a multiplexed proteomic approach in mice showed that the WAT is particularly susceptible to age-related changes, ranking among the most affected tissues [52]. Furthermore, we detected a significant positive correlation between the expression of *Il10*, *Il10ra* and *Il10rb* genes and aging, unique to gWAT. Given the direct role of IL-10 in the adipocyte homeostasis and thermogenesis [53,54], it is therefore possible that IL-10 might directly signal in adipocytes, synergizing with T cells in the WAT, and contributing to a faster phenotype in this tissue. We cannot however exclude other mechanisms such as preferential chemotaxis of the IL-10-reprogrammed T cells to gWAT. The alterations we report at the adipocyte level (decreased cell size, accumulation of cellular senescence) are in line with phenotypes described during accelerated aging, such as in progeria [55]. Since no correlation between the expression of *Il10*, *Il10ra* and *Il10rb* genes or the *Il10* signature and aging in the pancreas was detected, we hypothesize that the phenotype seen in the pancreas may be secondary to IL-10. One possibility is that it may result from an inflammatory spill-over from the adipose tissue. A recent study showed that pancreatic acinar cells were particularly enriched for senescent cells in aged mice, suggesting a high susceptibility of the exocrine pancreas to aging processes [56]. It is possible that prolonging the induction of IL-10 for longer periods may cause more widespread organismal effects, possibly with involvement of other organs.

We found that IL-10-accelerated aging is highly dependent on T cells and partially dependent on IFN-g. The importance of T cells in aging is well-established [20,30]. Given that IL-10-reprogrammed T cells share many features of aged T cells, their key role in the IL-10-mediated phenotype is expected. We have previously shown that IFN-g produced by T cells differentiated *in vivo* in the presence of high doses of IL-10 was required for the shift of the hematopoietic program towards emergency myelopoiesis [8]. Therefore, our findings show that although both IL-10-induced emergency myelopoiesis and accelerated aging are mediated by T cells, they differ in their dependency on IFN-g. Importantly, we found that IFN-g-deficient T cells preserve their transcriptomic and functional features in response to IL-10, suggesting that IFN-g-autocrine responses might not be central to drive T cell senescence. We also show that IFN-g deficiency did not compromise the accumulation of $PD1^{+}CD38^{+}$ T cells in non-lymphoid organs. Therefore, we speculate that IFN-g may be an important molecular cue to maximize retention of these senescent T cells in the tissues they home to and/or potentiate their production of granzymes or SASP known to mediate tissue damage [19,21]. It is also possible that IFN-g may itself promote tissue damage in a direct way, by initiating a senescence program in bystander cells, and therefore in its absence, a less or delayed effect of IL-10-reprogrammed T cells is observed. Of note, the transcriptome of IL-10-reprogramed $CD4^{+}$ and $CD8^{+}$ T cells showed an enrichment of *Gzmk*, which has been previously shown to contribute to non-immune cell senescence in tissues [19,21]. This molecule (and others) likely maintains the observed phenotype, partially compensating for the lack of IFN-g.

The finding that elevation of IL-10 drove T cell and systemic aging, led us to question whether this cytokine could also be involved in natural aging, as previously suggested [23,24,56]. By interrogating various available datasets, we confirmed that the IL-10-driven signature we observed is highly enriched in aged T cells and accumulates in different mouse tissues with age. Most interestingly, we found a positive correlation between *Il10*, *Il10ra* or *Il10rb* transcripts and the *Il10* signature with aging in the BM, spleen, gWAT, lung, kidney and brain. Thus, increased transcription of the *Il10* gene seems to accompany the accumulation of senescent T cells in different mouse tissues, implicating IL-10 as a novel immune mediator of aging. Importantly, simultaneous detection of IL-10 and T cells with an aged phenotype was also reported in COVID-19 patients [44] and in a subset of patients with CVID [43]. Furthermore, an increase in the levels of serum IL-10 and IFN-g was reported in human subjects as they age [24]. As we show here, an increase of IL-10 and of the IL-10 signature is also detected with age in humans, across different datasets [45,46]. Collectively these results indicate that, both in mouse and humans, a causal link between IL-10, hyperinflammation and immune senescence exists.

In summary, IL-10 elevation contributes to accelerated immunosenescence by acting via established causal key axes: reshaping the hematopoietic process towards myelopoiesis, as we showed before [8], and promoting T cell senescence, infiltration to non-lymphoid organs and disruption of tissue homeostasis. Our mouse model contributes to the expanding field of immunosenescence and inflammaging by showing that inflammation caused by persistent elevation of IL-10 levels in the absence of any infection or genetic defects, drives accelerated aging. Importantly, the general mechanisms of action of IL-10 [1] and many of the phenotypic characteristics of aged T cells are conserved in mice and humans [19]. Thus, our study brings

novel insights on the biology of IL-10 in natural aging, with broad implications for the design of IL-10 targeted therapies.

Methods

Ethics statement

All procedures involving mice were done in strict accordance with recommendations of the European Union Directive 2010/63/EU and previously approved by the Portuguese National Authority for Animal Health – *Direção Geral de Alimentação e Veterinária* (DGAV, ref. 012768/2021-09-13), and by the i3S Animal Welfare and Ethics Body or by the Pasteur Institute Safety Committee.

Mice

All mouse strains were on a C57BL/6 background. Age- and sex-matched mice were used for experiments (8–12 weeks old), and randomly assigned to experimental groups. All mice were bred and housed at i3S or Pasteur Institute and maintained under specific pathogen-conditions, in controlled temperature (20-24ºC), humidity (45-65%), and a light cycle of 12h (light/dark). Water and food were provided *ad libitum*. The pMT-10 mouse models used had been described before [8,29].

IL-10 induction

IL-10 overexpression was induced by administration of 50 mM zinc sulfate heptahydrate (ZnSO4.7H2O; Sigma-Aldrich) and 2% sucrose (Sigma-Aldrich) in the drinking water *ad libitum* for 30 days, as previously reported [8]. The mouse weight and any signs of distress were monitored over time.

Biological samples collection and cell suspension preparation

Mice were euthanized by increasing concentrations of carbon dioxide (CO_2) or by anesthetic overdose. Blood, BM, spleen, gWAT, colon, heart, lung, pancreas and liver were harvested, a fragment collected for histological analysis and immersed in neutral buffered formalin. For biochemical analysis, blood was collected by cardiac puncture under anesthesia (terminal bleeding). Single-cell suspensions from BM were obtained by flushing femurs and tibia with PBS 1X (Gibco, Thermo Fisher Scientific) supplemented with 2% FBS. Spleens were weighted for splenomegaly control [8] and single-cell suspensions were obtained by meshing total spleens in PBS 1X supplemented with 2% FBS. gWAT single cell suspensions were prepared by mincing the tissue with scissors followed by digestion with 1 mg/mL collagenase I (Sigma-Aldrich) and 50 µg/mL DNase (Roche) in RPMI buffer (Roche) at 37 ºC for 60 min. The digested tissue was filtered with a 70-µm cell strainer, followed by a 40-µm cell strainer. Colons were measured and excised longitudinally, washed and cut in pieces, prior to digestion in 2.5 mL of digestion buffer [DMEM (Roche) with 1 mM $CaCl_2$, 1 mM $MgCl_2$, and 1.5 mg/mL collagenase type IV (Roche)] followed by physical disruption and filtering through a 70 µm strainer. Leukocytes were separated by density gradient using Histopaque 1070. Lungs were aseptically excised after cardiac perfusion with PBS and digested using collagenase type IV (1 mg/mL; Roche) followed by physical disruption and filtering in a 70 µm strainer. For determining the lung

wet/dry ratio, left lungs were weighted and incubated at 60ºC for 72 h to remove water content. After this, lungs were again weighted, and water content calculated by subtracting the two values. Single cell suspensions from the heart were obtained by tissue dissociation with 600 U/mL collagenase II and 60 U/mL DNase I using a GentleMACs dissociator (Miltenyi Biotec, Cologne, Germany) as reported elsewhere [57]. When required, red blood cell lysis was performed with RBC lysis buffer (BioLegend). Live cells were counted in the different suspensions before further analyses.

Immunophenotyping by flow cytometry

Immune cell composition of different tissues was assessed by flow cytometry. 1-2 × 10^6 cells were washed and centrifuged at 300 x g for 3 minutes and all stained with Live/dead zombie fixable dye (Biolegend) to exclude dead cells. T cell profile in the BM, spleen, lung and colon was determined using the anti-mouse antibodies indicated in Supp Table 5. DNA damage was assessed by intranuclear staining with yH2AX Alexa Fluor 647 (clone N1-431). Cell fixation and permeabilization (fixation/permeabilization kit, eBiosciences) was performed after surface staining with specific antibodies as indicated in Supp Table 5. Mitochondrial mass and membrane potential were measured by labelling cell suspensions with 50 nM MitoTracker Green and 50 nM MitoTracker Red, respectively (both from Thermo Fisher Scientific). MitoTracker probes were diluted in pre-warmed (37º C) RPMI without serum and cells were incubated for 30 min at 37ºC. Data were acquired in a LSRFortessa flow cytometer (BD Biosciences). Post-acquisition analysis was performed using FlowJo™ v10.10 software (BD Biosciences). Representative plots are shown in Figure S1a.

Biochemical analysis

After collection, blood was allowed to clot for at least 30 minutes. Serum fraction was separated by centrifugation and serum parameters were blindly analysed in a certified laboratory (Cedivet, Portugal).

Histological evaluation

For histopathology examination, tissues were fixed in neutral buffered formalin for at least 24h, followed by routine processing and paraffin embedding. Consecutive 3 to 4 µm-thick sections were cut and stained with hematoxylin and eosin (H&E) and subsequently digitized using a high-throughput NanoZoomer 2.0HT Whole Slide Imager. Microscopic evaluation was performed by an experienced pathologist and an independent researcher, both blinded to the experimental protocol, based on the scoring system previously proposed by Orján et al. [38], with minor adaptations. A semi-quantitative grading system (0–8.5) was applied to assess pancreatic alterations: oedema was scored on a scale of 0–3 (0: none; 1: patchy interlobular; 2: diffuse interlobular; 3: diffuse interlobular and intra-acinar); leukocyte infiltration was scored on a scale of 0–5 (0: none; 1: patchy interlobular; 2: mild diffuse interlobular; 3: moderate diffuse interlobular; 4: diffuse interlobular and intra-acinar; 5: diffuse interlobular and intra-acinar with severe infiltration and acinar destruction). Presence of apoptotic cells was assigned with an additional 0.5 points. Leukocyte infiltration scores were compared between experimental groups. The average adipocyte area was quantified using the Adiposoft plugin of Fiji/ImageJ software. Hearts were included and sectioned transversally in consecutive sections spaced by 270 µm, as previously described [58]. One section from each series was stained with

Picrosirius Red and analyzed for interstitial fibrosis using a Leica DMI2000 brightfield microscope. A different section from each series was immunostained with alpha-sarcomeric actin antibody (Sigma Aldrich A2172), Alexa 568 goat anti-mouse IgM secondary antibody (Invitrogen A21043, 1:1000) and Wheat Germ Agglutinin (WGA, ThermoFischer W7024, 1:500) to assess cardiomyocyte area. Images were acquired in an Operetta CLS microscope (Revvity). Cardiomyocyte cross-sectional area was quantified in at least 100 transversely cut cardiomyocytes from each of the two most central heart sections using FIJI.

SA-β-galactosidase staining

SA-β-gal activity imaging was performed using a SA-β-gal staining kit (Cell Signaling Technology), according to the manufacturer's instructions. SA-β-gal activity detection by flow cytometry was done using Fluorescein di-β-galactopyranoside (ThermoFisher), accordingly with manufacturer's instructions. For flow cytometry, cells were additionally stained with specific antibodies as indicated in Supp Table 5. Representative plots are shown in Figure S1a.

Transmission electron microscopy

Live $CD3^+CD4^+$ and $CD3^+CD8^+$ T cells were sorted through a FACS Aria II (BD Biosciences). Isolated cells were activated with 0.2 µg plate-bound anti-mouse CD3 (clone 145-2C11) and 0,8 µg soluble anti-CD28 (clone 37.51), both from BioLegend, during 24h at 37ºC, 5% CO_2. For ultrastructural analysis, cells were fixed overnight at 4°C in 2% formaldehyde and 2.5% glutaraldehyde in 0.1 M sodium cacodylate buffer. Cells were then washed with 0.1 M sodium cacodylate buffer, embedded in Histogel™, and post-fixed for 1 hour in 1% osmium tetroxide and 1.5% potassium ferrocyanide in 0.1 M sodium cacodylate buffer. Afterward, the cells were stained overnight with aqueous 2% uranyl acetate at 4°C, dehydrated with ethanol, and embedded in Embed-812 resin. Ultra-thin sections (70 nm thick) were cut using an RMC Ultramicrotome with Diatome diamond knives, mounted on 200 mesh copper grids, and stained with uranyless and 3% lead citrate for 5 minutes each, with washes between steps. Imaging was done using a JEOL JEM 1400 transmission electron microscope, and digital images were captured with a PHURONA CCD camera. Transmission electron microscopy was performed at the HEMS core facility at i3S, University of Porto, Portugal. Three to fifteen cells from each case were analysed and preserved mitochondria were counted per cell according to the presence of double membrane with inner membrane folds known as cristae.

RNA isolation, sequencing and bioinformatics analyses

$CD3^+CD4^+$ and $CD3^+CD8^+$ T cells were sort-purified as before [8] from pMT-10 mice competent or deficient for the IL-10Ra chain or IFN-g, induced or not to over-express IL-10. Sorted samples were isolated directly into lysis buffer of RNeasy Micro Kit and kept at -80ºC until RNA extraction. Targeted RNA sequencing was performed by GenCore, i3S (Instituto de Investigação e Inovação em Saúde) using the Ion AmpliSeq Transcriptome Mouse Gene Expression Kit (ThermoFisher), which covers over 20,000 mouse RefSeq genes. Data were processed using the Ion Torrent platform specific pipeline software Torrent Suite v5.18 to generate sequence reads, trim adapter sequences, filter and remove poor signal reads, and split the reads according to the barcode. FASTQ and/or BAM files were generated using the Torrent Suit plugin

FileExporter v5.18. Primary automated analysis for AmpliSeq sequencing data of all samples was performed using the ampliSeqRNA plugin v.5.18 (target region "AmpliSeq_Mouse_Transcriptome_V1_Designed"). Plugin reports normalized transcript counts in spreadsheet file formats.

Data was analysed using R version 4.3.0. Raw counts were normalized using the quantile method, and denoising was performed with the noisyR package (version 1.0.0) [59]. The bulkanalysR package (version 1.12.0) was used for analysis and visualization of the data [59]. Differential expression analysis was conducted using the edgeR package [60]. Genes were identified as significant using a threshold of an adjusted p value < 0.05 (Benjamini-Hochberg method) and an absolute log2 fold-change cutoff of >=2. Heatmaps were created using the ComplexHeatmap package (version 2.16.0).

Gene Set Enrichment Analysis (GSEA) of Hallmark Pathways

To identify enriched biological pathways, we performed GSEA on four selected conditions ($CD4^+$ and $CD8^+$ T cells analyses for pMT-10 and pMT-10.$IFNg^{-/-}$ both plus vs minus Zn). Genes were ranked by $\log_2$ fold-change, and enrichment was assessed using the clusterProfiler package (v4.10.1) in R, with Hallmark gene sets (MSigDB v2023.1, “H” collection) retrieved via the msigdbr package (v10.0.1) for *Mus musculus*. For each dataset, enrichment scores were calculated using permutation-based testing (1000 permutations), and false discovery rate (FDR)-adjusted *p* values were reported. Gene sets with FDR < 0.05 were considered significant.

For visualization, the top 50 positively and 50 negatively enriched pathways per condition were selected based on normalized enrichment score (NES). Dot plots were generated using ggplot2 (v3.5.1), with point size representing $-\log_{10}(padj)$ and color indicating NES. All data wrangling and plotting were conducted using dplyr (v1.1.4) and supporting packages.

Il10 Signature Score Calculation

A custom 16-gene (*Ccl3, Ccl4, Ccl5, Il10, Gzmk, Gzmb, Cd38, Eomes, Lag3, Tox2, Pdcd1, Tigit, Prf1, Cdkn1a, Cdkn2a,* and *Ccna2*) *Il10* signature was used for correlation tests and visualization. This signature was derived from the 21-genes selected for initial analyses, based on a log2FC≥1 and adjusted p value≤0.05 in at least one of the analysed T cell subsets (Supp Tables 1 and 2). The *Ifng* gene was not included in the *Il10* signature as the phenotype observed upon IL-10 induction does not fully require IFN-g (see Figure 3). The signature score was calculated as the mean of the log2-transformed expression values of the 16 genes.

Il10 Signature Gene Set Enrichment Analysis (GSEA)

To evaluate the enrichment of the T-cell immune-regulatory transcriptional program, GSEA was applied to differential experimental conditions using the fgsea package (v1.28.0). Genes were independently ranked for each condition by their $\log_2$ fold-change, and GSEA was performed separately for upregulated (positive) and downregulated (negative) genes using fgseaMultilevel with minimum and maximum pathway sizes set

to 5 and 500, respectively. Enrichment was computed using a directional scoring approach (scoreType = "pos" and "neg"), and results were retained if the adjusted *p*-value (Benjamini-Hochberg correction) was < 0.05. NES were extracted and visualized using standard lollipop plots implemented in ggplot2 (v3.5.1), with NES magnitude encoded by point size and statistical significance by $-\log_{10}(p\text{adj})$ color gradients. Enrichment plots were also generated to visually depict the enrichment score for each condition-specific ranked gene list. The same work-flow was applied to GSEA of the *Il10* signature with previously established transcriptomic signatures of aging [39] and lifespan-extending interventions [42]. Signatures of aging [39] included genes found differentially expressed (DEGs) in aged mouse tissues (multi-tissue or liver-specific signatures). Signatures of lifespan-extending interventions [42] (LEI) included DEGs found in the liver in response to cellular reprogramming and associated with longevity interventions (caloric restriction, rapamycin, growth hormone deficiency) effect on mouse maximum and median lifespan. These signatures were extracted
from https://github.com/shappiron/Reprogramming_meta/blob/main/signatures/Aging%3AMouse.csv and used in [39,42].

Correlation of *Il10* Signature Expression with Age Across Mouse Tissues

Normalized gene expression data ($\log_2$-transformed counts) were obtained from the *Tabula Muris Senis* bulk RNA-seq dataset. Expression values were extracted for the custom *Il10* signature (see above) and compared against age across multiple tissues. Both *Il10* signature (n = 16 genes) and *Il10* alone were analyzed. For each analysis, expression data were filtered by tissue and age, and Pearson correlation coefficients were calculated between age and gene expression using cor.test in R (stats package, v4.3.2). Correlation analyses were stratified into "main" (marrow, spleen, pancreas, gWAT) and "supplementary" (e.g., brain, lung, liver) tissue groups. Tissue-specific correlation values (*r*) and associated *p*-values were reported. Visualization was performed using ggplot2 (v3.5.1), with loess-smoothed regression curves fit separately for each tissue. Correlation coefficients were annotated directly on each panel, and tissues were ordered by relevance. This approach enabled assessment of age-related transcriptional dynamics of the *Il10* and *Il10* signature.

Cell-specific gene expression patterns of the *Il10* signature during murine aging was investigated using the single-cell RNA sequencing (scRNA-seq) data from the *Tabula Muris Senis* FACS dataset [61]. Pre-processed .rds files (https://cellxgene.cziscience.com/collections) were imported into Seurat [62] (v5.1.0) in R, and gene counts were normalized using the NormalizeData function using default parameters. Then, the global *Il10* signature score (n = 16 genes) was computed for each cell using the UCell package [63] (v2.8.0). For each tissue and age, UMAP plots containing signature scores for individual cells were then generated.

Profiling of *Il10* Signature Expression with Age in Human Immune Cells

The expression of the *Il10* signature in human aged immune cells was analysed using previously curated public scRNA-seq datasets of human immune aging [46]. Mouse gene symbols were converted to their corresponding human orthologues using gProfiler2 [64]. For each gene, changes in expression along aging were obtained for each cell type in the bone marrow, blood and spleen. The enrichment of the *Il10* signature

with age for each cell type in each tissue was analyzed using GSEA, with an adjusted *p*-value (Benjamini-Hochberg correction) < 0.1 considered to be significant. To investigate T cell-specific gene expression patterns of the *Il10* signature during human aging, pre-processed .h5ad files (https://cellxgene.cziscience.com/collections) were converted to Seurat objects using zellkonverter (1.18) and imported into Seurat (v5.1.0) in R. Then, the global *Il10* signature score using human orthologues was computed for each cell using the UCell package (v2.8.0). For each tissue, age group and T cell type, UMAP plots containing signature scores for single cells were generated.

DNA methylation aging clock

Genomic DNA was extracted from blood collected by cardiac puncture into ethylenediamine tetraacetic acid (EDTA)-treated tubes (BD Vacutainer®). The extraction was performed using a commercial kit (QIamp DNA Blood purification kit from Qiagen), following the manufacturer's instructions, and the resulting DNA was quantified with Qubit. 250 ng of extracted DNA were sent to the non-profit Epigenetic Clock Foundation for the assessment of DNA methylation clocks using the custom mammalian array (HorvathMammalMethylChip40).

Data availability

The T cell targeted RNA-seq of $CD4^+$ and $CD8^+$ T cells from C57BL/6 and pMT-10 mice fed with control or Zn-enriched water has been published before [8] and available at NCBI Gene Expression Omnibus (GSE172060). The sequencing datasets generated for the current study have been submitted to the GEO repository and will be made available upon request during revision, and publicly released upon publication. All other data are available from the corresponding authors upon reasonable request.

Statistical analysis

All data were analysed with the GraphPad Prism software (v.9, GraphPad software Inc. 455 CA). Results are presented as means ± standard errors of the means (s.e.m.). Sample sizes and statistical tests are discriminated in each figure legend. Exact p-values are shown in each figure. No statistical methods were used to predetermine sample size. Data collection and analysis were not performed blinded to the conditions of the experiments.

Declarations

Author contributions

Conceptualization: ACM, RFS, IF, JPC, IC, AGC, PV, EL, MS

Formal analysis: ACM, RFS, IF, JPC, RG, CSS, NSO, SP, IA, EG, RS, DSN

Funding Acquisition: PV, EL, MS

Investigation: ACM, RFS, IF, RG, MSC, ENG, RDS

Project administration: PV, EL, MS

Resources: JPC, CSS, NSO

Supervision: PV, EL, MS

Visualization: RFS, IF, JPC, CSS, NSO, PV, EL, MS

Writing of the draft: JPC, AGC, PV, EL, MS

Writing-review and editing: all authors

Competing interests

The authors declare no competing interests.

Acknowledgements

The authors thank the support from the Instituto de Investigação e Inovação em Saúde scientific platforms animal facility, histology and electron microscopy and translational cytometry. This work is a result of the project NORTE2030-FEDER-01777300 - SCALE-ImmunoHUB2030, supported by Norte Portugal Regional Operational Programme (NORTE 2030), under the PORTUGAL 2030 Partnership Agreement, through the European Regional Development Fund (FEDER) and was also supported by the *Institut Pasteur*. ACM, IF, RG and CSS were funded by PhD grants SFRH/BD/136800/2016, 2024.02516.BD, 2022.12852.BD and UI/BD/154458/2022 from FCT. JPC was funded by FCT (2022.00872.CEECIND). EL was funded by the FCT grant 2020.00654.CEECIND; by FCT, FEDER (Fundo Europeu de Desenvolvimento Regional) through COMPETE 2020 – Operational Program for Competitiveness and Internationalization (POCI), Portugal 2020, Grant PTDC/MED-OUT/2747/2020; by FCT, FEDER through COMPETE 2030, Portugal 2030, Grant COMPETE2030-FEDER-00704600; and by Maximon AG, Switzerland, Maximon Longevity Prize 2022.

References

1. Moore, K. W., de Waal Malefyt, R., Coffman, R. L. & O'Garra, A. Interleukin-10 and the interleukin-10 receptor. *Annu Rev Immunol* **19**, 683-765 (2001). https://doi.org:10.1146/annurev.immunol.19.1.683
2. Saraiva, M., Vieira, P. & O'Garra, A. Biology and therapeutic potential of interleukin-10. *J Exp Med* **217** (2020). https://doi.org:10.1084/jem.20190418
3. van Deventer, S. J., Elson, C. O. & Fedorak, R. N. Multiple doses of intravenous interleukin 10 in steroid-refractory Crohn's disease. Crohn's Disease Study Group. *Gastroenterology* **113**, 383-389 (1997). https://doi.org:10.1053/gast.1997.v113.pm9247454
4. Huhn, R. D. *et al.* Effects of single intravenous doses of recombinant human interleukin-10 on subsets of circulating leukocytes in humans. *Immunopharmacology* **41**, 109-117 (1999). https://doi.org:10.1016/s0162-3109(98)00058-7
5. Sosman, J. A. *et al.* Interleukin 10-induced thrombocytopenia in normal healthy adult volunteers: evidence for decreased platelet production. *Br J Haematol* **111**, 104-111 (2000).

https://doi.org:10.1046/j.1365-2141.2000.02314.x

6. Tilg, H., Ulmer, H., Kaser, A. & Weiss, G. Role of IL-10 for induction of anemia during inflammation. *J Immunol* **169**, 2204-2209 (2002). https://doi.org:10.4049/jimmunol.169.4.2204
7. Tilg, H. *et al.* Treatment of Crohn's disease with recombinant human interleukin 10 induces the proinflammatory cytokine interferon gamma. *Gut* **50**, 191-195 (2002). https://doi.org:10.1136/gut.50.2.191
8. Cardoso, A. *et al.* Interleukin-10 induces interferon-gamma-dependent emergency myelopoiesis. *Cell Rep* **37**, 109887 (2021). https://doi.org:10.1016/j.celrep.2021.109887
9. Kanayama, M. *et al.* Myeloid-like B cells boost emergency myelopoiesis through IL-10 production during infection. *J Exp Med* **220** (2023). https://doi.org:10.1084/jem.20221221
10. Tang, Y. *et al.* Excessive IL-10 and IL-18 trigger hemophagocytic lymphohistiocytosis-like hyperinflammation and enhanced myelopoiesis. *J Allergy Clin Immunol* **150**, 1154-1167 (2022). https://doi.org:10.1016/j.jaci.2022.06.017
11. Collins, A. *et al.* Maternal inflammation regulates fetal emergency myelopoiesis. *Cell* **187**, 1402-1421 e1421 (2024). https://doi.org:10.1016/j.cell.2024.02.002
12. Chang, Y. W. *et al.* A CSF-1R-blocking antibody/IL-10 fusion protein increases anti-tumor immunity by effectuating tumor-resident CD8(+) T cells. *Cell Rep Med* **4**, 101154 (2023). https://doi.org:10.1016/j.xcrm.2023.101154
13. Emmerich, J. *et al.* IL-10 directly activates and expands tumor-resident CD8(+) T cells without de novo infiltration from secondary lymphoid organs. *Cancer Res* **72**, 3570-3581 (2012). https://doi.org:10.1158/0008-5472.CAN-12-0721
14. Mumm, J. B. *et al.* IL-10 elicits IFNgamma-dependent tumor immune surveillance. *Cancer Cell* **20**, 781-796 (2011). https://doi.org:10.1016/j.ccr.2011.11.003
15. Naing, A. *et al.* PEGylated IL-10 (Pegilodecakin) Induces Systemic Immune Activation, CD8(+) T Cell Invigoration and Polyclonal T Cell Expansion in Cancer Patients. *Cancer Cell* **34**, 775-791 e773 (2018). https://doi.org:10.1016/j.ccell.2018.10.007
16. Yogev, N. *et al.* CD4(+) T-cell-derived IL-10 promotes CNS inflammation in mice by sustaining effector T cell survival. *Cell Rep* **38**, 110565 (2022). https://doi.org:10.1016/j.celrep.2022.110565
17. Hanna, B. S. *et al.* Interleukin-10 receptor signaling promotes the maintenance of a PD-1(int) TCF-1(+) CD8(+) T cell population that sustains anti-tumor immunity. *Immunity* **54**, 2825-2841 e2810 (2021). https://doi.org:10.1016/j.immuni.2021.11.004
18. Elyahu, Y. *et al.* Aging promotes reorganization of the CD4 T cell landscape toward extreme regulatory and effector phenotypes. *Sci Adv* **5**, eaaw8330 (2019). https://doi.org:10.1126/sciadv.aaw8330
19. Mogilenko, D. A. *et al.* Comprehensive Profiling of an Aging Immune System Reveals Clonal GZMK(+) CD8(+) T Cells as Conserved Hallmark of Inflammaging. *Immunity* **54**, 99-115 e112 (2021). https://doi.org:10.1016/j.immuni.2020.11.005
20. Soto-Heredero, G., Gomez de Las Heras, M. M., Escrig-Larena, J. I. & Mittelbrunn, M. Extremely Differentiated T Cell Subsets Contribute to Tissue Deterioration During Aging. *Annu Rev Immunol* **41**,

181-205 (2023). https://doi.org:10.1146/annurev-immunol-101721-064501

21. Desdin-Mico, G. *et al.* T cells with dysfunctional mitochondria induce multimorbidity and premature senescence. *Science* **368**, 1371-1376 (2020). https://doi.org:10.1126/science.aax0860
22. Yousefzadeh, M. J. *et al.* An aged immune system drives senescence and ageing of solid organs. *Nature* **594**, 100-105 (2021). https://doi.org:10.1038/s41586-021-03547-7
23. Almanan, M. *et al.* IL-10-producing Tfh cells accumulate with age and link inflammation with age-related immune suppression. *Sci Adv* **6**, eabb0806 (2020). https://doi.org:10.1126/sciadv.abb0806
24. Lustig, A. *et al.* Telomere Shortening, Inflammatory Cytokines, and Anti-Cytomegalovirus Antibody Follow Distinct Age-Associated Trajectories in Humans. *Front Immunol* **8**, 1027 (2017). https://doi.org:10.3389/fimmu.2017.01027
25. Lio, D. *et al.* Gender-specific association between -1082 IL-10 promoter polymorphism and longevity. *Genes Immun* **3**, 30-33 (2002). https://doi.org:10.1038/sj.gene.6363827
26. Cauley, J. A. *et al.* Inflammatory Markers and the Risk of Hip and Vertebral Fractures in Men: the Osteoporotic Fractures in Men (MrOS). *J Bone Miner Res* **31**, 2129-2138 (2016). https://doi.org:10.1002/jbmr.2905
27. Neves, J. & Sousa-Victor, P. Regulation of inflammation as an anti-aging intervention. *FEBS J* **287**, 43-52 (2020). https://doi.org:10.1111/febs.15061
28. Westbrook, R. M. *et al.* Aged interleukin-10tm1Cgn chronically inflamed mice have substantially reduced fat mass, metabolic rate, and adipokines. *PLoS One* **12**, e0186811 (2017). https://doi.org:10.1371/journal.pone.0186811
29. Cardoso, A. *et al.* The Dynamics of Interleukin-10-Afforded Protection during Dextran Sulfate Sodium-Induced Colitis. *Front Immunol* **9**, 400 (2018). https://doi.org:10.3389/fimmu.2018.00400
30. Mittelbrunn, M. & Kroemer, G. Hallmarks of T cell aging. *Nat Immunol* **22**, 687-698 (2021). https://doi.org:10.1038/s41590-021-00927-z
31. Kell, L., Simon, A. K., Alsaleh, G. & Cox, L. S. The central role of DNA damage in immunosenescence. *Front Aging* **4**, 1202152 (2023). https://doi.org:10.3389/fragi.2023.1202152
32. Martinez-Zamudio, R. I. *et al.* Senescence-associated beta-galactosidase reveals the abundance of senescent CD8+ T cells in aging humans. *Aging Cell* **20**, e13344 (2021). https://doi.org:10.1111/acel.13344
33. Pieren, D. K. J. *et al.* Compromised DNA Repair Promotes the Accumulation of Regulatory T Cells With an Aging-Related Phenotype and Responsiveness. *Front Aging* **2** (2021). https://doi.org:10.3389/fragi.2021.667193
34. Haghani, A. *et al.* DNA methylation networks underlying mammalian traits. *Science* **381**, eabq5693 (2023). https://doi.org:10.1126/science.abq5693
35. Ying, K. *et al.* Causality-enriched epigenetic age uncouples damage and adaptation. *Nat Aging* **4**, 231-246 (2024). https://doi.org:10.1038/s43587-023-00557-0
36. Frasca, D. & Blomberg, B. B. Adipose tissue, immune aging, and cellular senescence. *Semin Immunopathol* **42**, 573-587 (2020). https://doi.org:10.1007/s00281-020-00812-1

37. Kirkland, J. L. & Dobson, D. E. Preadipocyte function and aging: links between age-related changes in cell dynamics and altered fat tissue function. *J Am Geriatr Soc* **45**, 959-967 (1997). https://doi.org:10.1111/j.1532-5415.1997.tb02967.x
38. Orjan, E. M. *et al.* The anti-inflammatory effect of dimethyl trisulfide in experimental acute pancreatitis. *Sci Rep* **13**, 16813 (2023). https://doi.org:10.1038/s41598-023-43692-9
39. Tyshkovskiy, A. *et al.* Distinct longevity mechanisms across and within species and their association with aging. *Cell* **186**, 2929-2949 e2920 (2023). https://doi.org:10.1016/j.cell.2023.05.002
40. Palovics, R. *et al.* Molecular hallmarks of heterochronic parabiosis at single-cell resolution. *Nature* **603**, 309-314 (2022). https://doi.org:10.1038/s41586-022-04461-2
41. Tabula Muris, C. *et al.* Single-cell transcriptomics of 20 mouse organs creates a Tabula Muris. *Nature* **562**, 367-372 (2018). https://doi.org:10.1038/s41586-018-0590-4
42. Tyshkovskiy, A. *et al.* Identification and Application of Gene Expression Signatures Associated with Lifespan Extension. *Cell Metab* **30**, 573-593 e578 (2019). https://doi.org:10.1016/j.cmet.2019.06.018
43. Stuchly, J. *et al.* Common Variable Immunodeficiency patients with a phenotypic profile of immunosenescence present with thrombocytopenia. *Sci Rep* **7**, 39710 (2017). https://doi.org:10.1038/srep39710
44. Diao, B. *et al.* Reduction and Functional Exhaustion of T Cells in Patients With Coronavirus Disease 2019 (COVID-19). *Front Immunol* **11**, 827 (2020). https://doi.org:10.3389/fimmu.2020.00827
45. Goeminne, L. J. E. *et al.* Plasma protein-based organ-specific aging and mortality models unveil diseases as accelerated aging of organismal systems. *Cell Metab* **37**, 205-222 e206 (2025). https://doi.org:10.1016/j.cmet.2024.10.005
46. Wells, S. B. *et al.* Multimodal profiling reveals tissue-directed signatures of human immune cells altered with age. *Nat Immunol* **26**, 1612-1625 (2025). https://doi.org:10.1038/s41590-025-02241-4
47. Li, X. *et al.* Inflammation and aging: signaling pathways and intervention therapies. *Signal Transduct Target Ther* **8**, 239 (2023). https://doi.org:10.1038/s41392-023-01502-8
48. Widjaja, A. A. *et al.* Inhibition of IL-11 signalling extends mammalian healthspan and lifespan. *Nature* **632**, 157-165 (2024). https://doi.org:10.1038/s41586-024-07701-9
49. Hashimoto, K. *et al.* Single-cell transcriptomics reveals expansion of cytotoxic CD4 T cells in supercentenarians. *Proc Natl Acad Sci U S A* **116**, 24242-24251 (2019). https://doi.org:10.1073/pnas.1907883116
50. Jin, J. *et al.* CISH impairs lysosomal function in activated T cells resulting in mitochondrial DNA release and inflammaging. *Nat Aging* **3**, 600-616 (2023). https://doi.org:10.1038/s43587-023-00399-w
51. Schaum, N. *et al.* Ageing hallmarks exhibit organ-specific temporal signatures. *Nature* **583**, 596-602 (2020). https://doi.org:10.1038/s41586-020-2499-y
52. Yu, Q. *et al.* Sample multiplexing for targeted pathway proteomics in aging mice. *Proc Natl Acad Sci U S A* **117**, 9723-9732 (2020). https://doi.org:10.1073/pnas.1919410117
53. Rajbhandari, P. *et al.* Single cell analysis reveals immune cell-adipocyte crosstalk regulating the transcription of thermogenic adipocytes. *Elife* **8** (2019). https://doi.org:10.7554/eLife.49501

54. Rajbhandari, P. *et al.* IL-10 Signaling Remodels Adipose Chromatin Architecture to Limit Thermogenesis and Energy Expenditure. *Cell* **172**, 218-233 e217 (2018). https://doi.org:10.1016/j.cell.2017.11.019
55. Ribeiro, R. *et al.* In vivo cyclic induction of the FOXM1 transcription factor delays natural and progeroid aging phenotypes and extends healthspan. *Nat Aging* **2**, 397-411 (2022). https://doi.org:10.1038/s43587-022-00209-9
56. Sanborn, M. A., Wang, X., Gao, S., Dai, Y. & Rehman, J. Unveiling the cell-type-specific landscape of cellular senescence through single-cell transcriptomics using SenePy. *Nat Commun* **16**, 1884 (2025). https://doi.org:10.1038/s41467-025-57047-7
57. Sampaio-Pinto, V. *et al.* Neonatal Apex Resection Triggers Cardiomyocyte Proliferation, Neovascularization and Functional Recovery Despite Local Fibrosis. *Stem Cell Reports* **10**, 860-874 (2018). https://doi.org:10.1016/j.stemcr.2018.01.042
58. Valente, M. *et al.* Optimized Heart Sampling and Systematic Evaluation of Cardiac Therapies in Mouse Models of Ischemic Injury: Assessment of Cardiac Remodeling and Semi-Automated Quantification of Myocardial Infarct Size. *Curr Protoc Mouse Biol* **5**, 359-391 (2015). https://doi.org:10.1002/9780470942390.mo140293
59. Moutsopoulos, I. *et al.* noisyR: enhancing biological signal in sequencing datasets by characterizing random technical noise. *Nucleic Acids Res* **49**, e83 (2021). https://doi.org:10.1093/nar/gkab433
60. Love, M. I., Huber, W. & Anders, S. Moderated estimation of fold change and dispersion for RNA-seq data with DESeq2. *Genome Biol* **15**, 550 (2014). https://doi.org:10.1186/s13059-014-0550-8
61. Tabula Muris, C. A single-cell transcriptomic atlas characterizes ageing tissues in the mouse. *Nature* **583**, 590-595 (2020). https://doi.org:10.1038/s41586-020-2496-1
62. Hao, Y. *et al.* Dictionary learning for integrative, multimodal and scalable single-cell analysis. *Nat Biotechnol* **42**, 293-304 (2024). https://doi.org:10.1038/s41587-023-01767-y
63. Andreatta, M. & Carmona, S. J. UCell: Robust and scalable single-cell gene signature scoring. *Comput Struct Biotechnol J* **19**, 3796-3798 (2021). https://doi.org:10.1016/j.csbj.2021.06.043
64. Kolberg, L., Raudvere, U., Kuzmin, I., Vilo, J. & Peterson, H. gprofiler2 -- an R package for gene list functional enrichment analysis and namespace conversion toolset g:Profiler. *F1000Res* **9** (2020). https://doi.org:10.12688/f1000research.24956.2

Figures

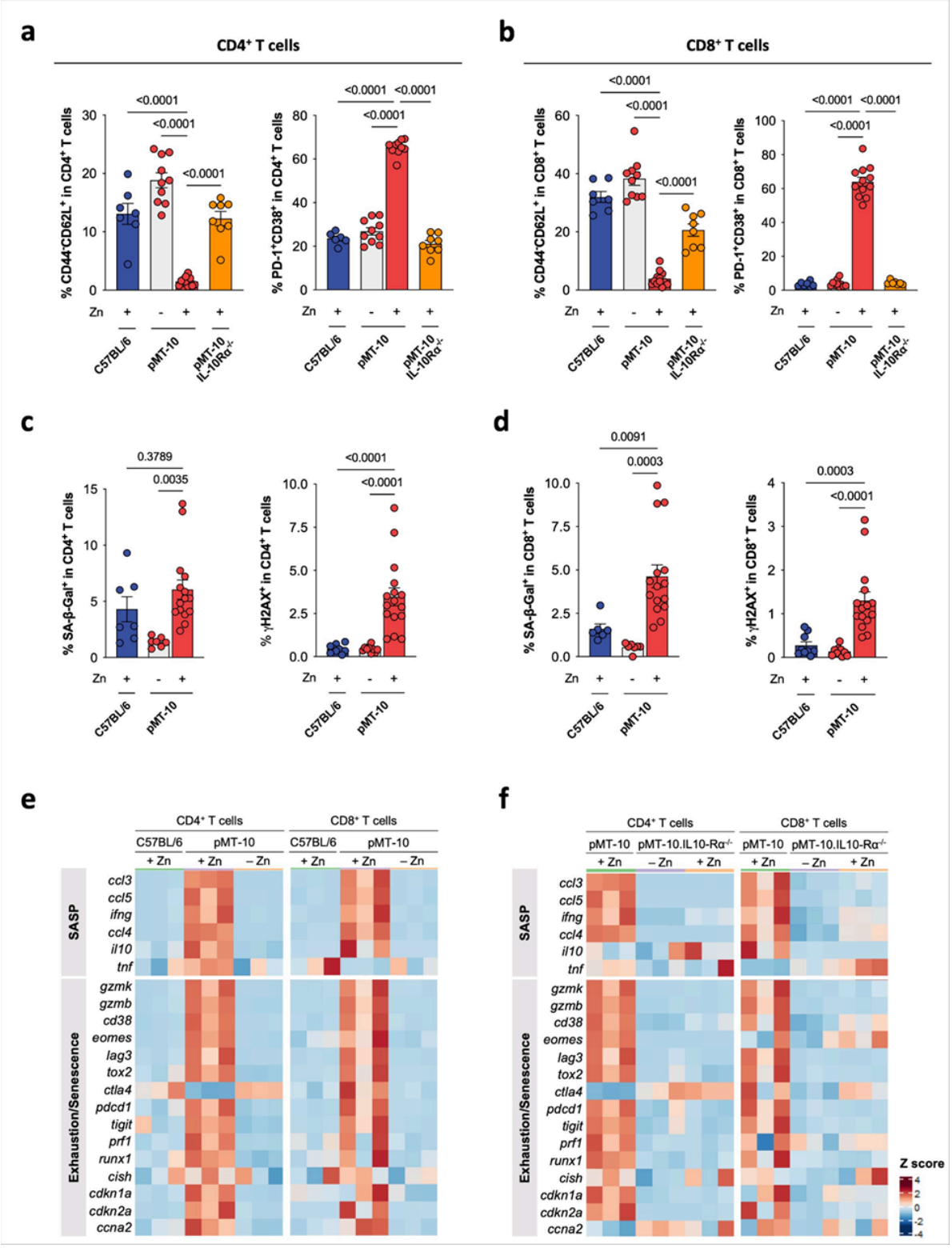


Figure 1

IL-10 induces bone marrow T cell senescence *in vivo.* C57BL/6, pMT10 or pMT10.IL-10Ra deficient ($^{-/-}$) mice were fed for 30 days with control (–) or Zn-enriched (+) water and at that time-point the CD4 and CD8 T cell populations analyzed in the bone marrow. (**a-d**) Flow cytometry of $CD4^+$ (a, c) and $CD8^+$ (b, d) T cell populations analysing the frequency of naïve ($CD44^-$ $CD62L^+$) and activated $PD\text{-}1^+$ $CD38^+$ T cells (a, b) and of SA-β-gal^+ and $γH2AX^+$ T cells (c, d) in each group of mice. Bars represent the mean ± s.e.m for 6 – 16

mice, from 1 – 5 independent experiments, and each dot represents a single mouse. One-way ANOVA tests were used to identify statistical differences between two groups. *p* values are shown for the different comparisons. (**e, f**) Heatmap representation showing the relative expression of genes encoding the indicated SASP and T cell exhaustion/senescence markers in $CD4^+$ and $CD8^+$ T cells sort-purified from the bone marrow of pMT-10+Zn (e) or pMT10.IL-$10Ra^{-/-}$+Zn (f) versus the indicated control mice. Each row represents one mouse.

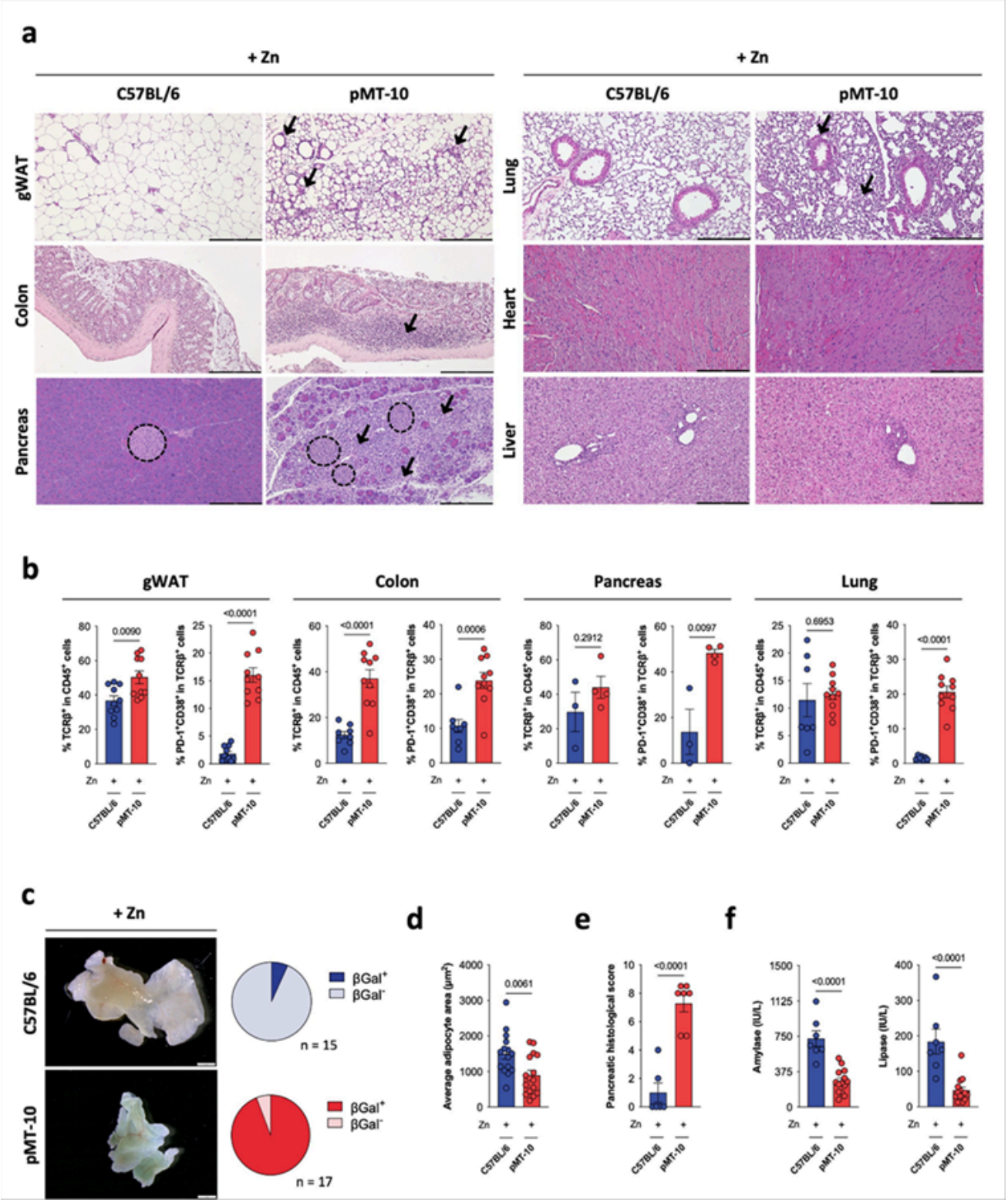


Figure 2

IL-10 elevation causes structural and functional alterations in multiple non-lymphoid organs. C57BL/6 and pMT10 mice were fed for 30 days with Zn-enriched water and at that time-point several organs were analysed. (**a**) Representative microscopic images of hematoxylin and eosin-stained sections of the indicated tissues (40X magnification; scale bar, 250 μm). Arrows indicate cellular infiltrates and dotted circles β-islets. (**b**) Frequency of $TCR\beta^+$ in $CD45^+$ cells and of activated $PD\text{-}1^+$ $CD38^+$ T cells determined by flow cytometry in gonadal white adipose tissue (gWAT), colon, pancreas and lung. (**c**) Representative images of gWAT from pMT-10 or control (C57BL/6) mice stained for SA-β-gal activity (0.8X magnification; scale bar, 2 mm) and the respective quantification of β-gal positive (+) or negative (-) samples for the total (n) mice tested. Quantification of the average adipocyte area (**d**), and pancreatic histological score (**e**) from the hematoxylin and eosin images obtained for each mouse. (**f**) Detection of amylase and lipase in the serum of the indicated animals. (b, d-f) Bars represent the mean ± s.e.m. for 3 – 16 mice, from 1 – 5 independent experiments. Each dot represents a single mouse. Data were analyzed with Student's t test. *p* values are shown for the indicated comparisons.

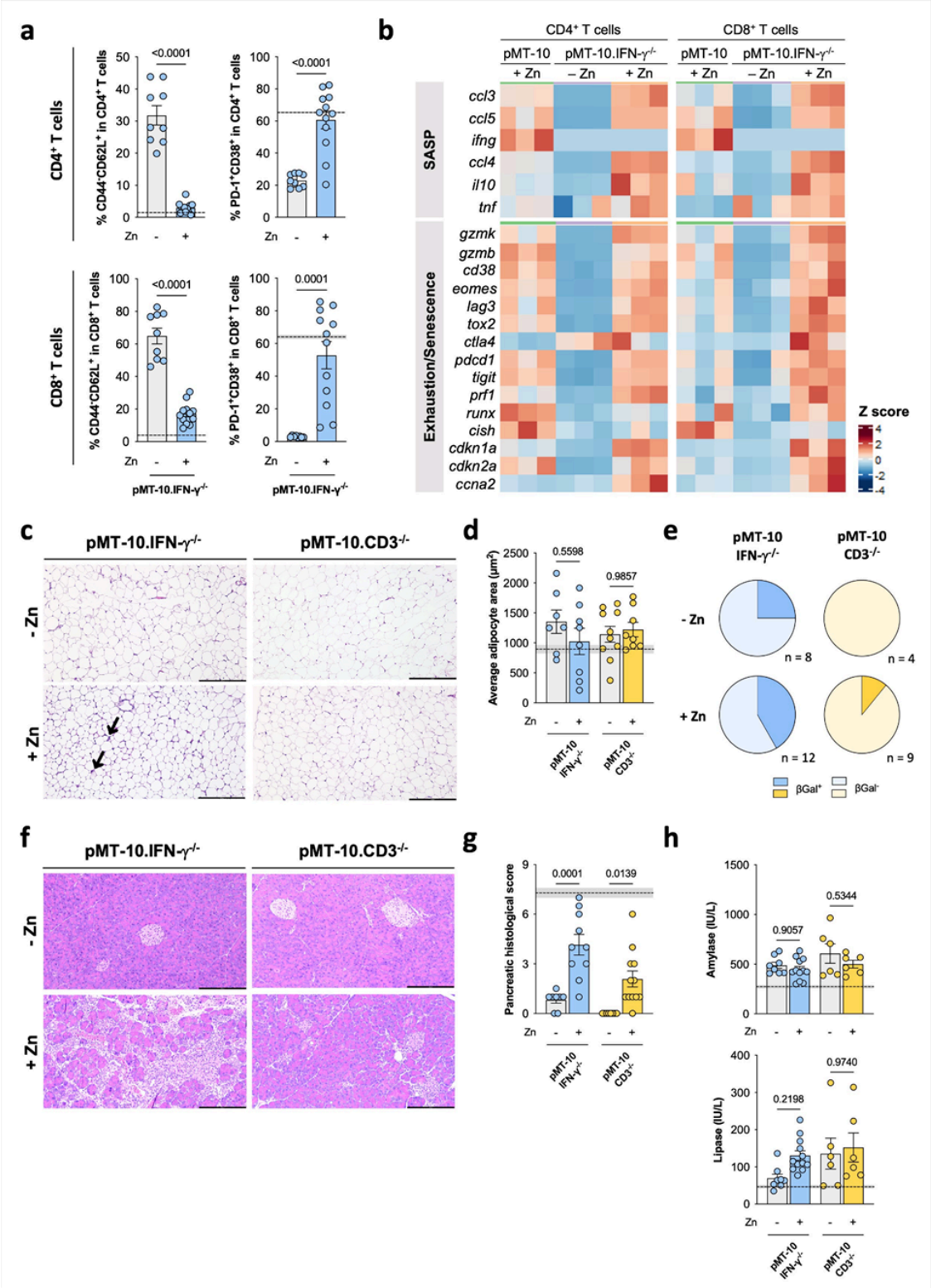


Figure 3

IL-10-induced progeroid features in the adipose tissue and pancreas are T cell-dependent. Groups of pMT-10 mice of the indicated phenotypes were fed with control (–) or Zn-enriched (+) water for 30 days. (**a**) Frequency of naïve ($CD44^-CD62L^+$) and $PD\text{-}1^+CD38^+$ activated $CD4^+$ and CD8+ T cells in the bone marrow determined by flow cytometry. (**b**) Heatmap representation showing the relative expression of genes encoding the indicated SASP and T cell exhaustion/senescence markers in $CD4^+$ and $CD8^+$ T cells sort-

purified from the bone marrow of the indicated mice. Each row represents one mouse. (**c**) Representative microscopic images of hematoxylin and eosin-stained sections of gonadal white adipose tissue (gWAT) of induced or control pMT-10.IFNg$^{-/-}$ and pMT-10.CD3$^{-/-}$ mice (40X magnification; scale bar, 250 μm). Arrows point at cellular infiltrates. Quantification of the average adipocyte area (**d**) and of SA-β-gal positivity (**e**) detected for gonadal adipose tissue of the indicated mouse phenotypes. (**f**) Representative microscopic images of hematoxylin and eosin-stained sections of pancreas of induced or control pMT-10.IFNg$^{-/-}$ and pMT-10.CD3$^{-/-}$ mice (40X magnification; scale bar, 250 μm). Quantification of (**g**) pancreatic damage using an established pancreatic histological score and (**h**) alterations in serum enzyme levels. (a, d, g, h) Bars represent the mean ± s.e.m. for 6 – 12 mice, from 4 – 6 independent experiments. Each dot represents a single mouse. For comparison, dashed lines represent the mean ± s.e.m. obtained for pMT-10 + Zn mice. Data were analyzed with Student's t test. *p* values are shown for the indicated comparisons.

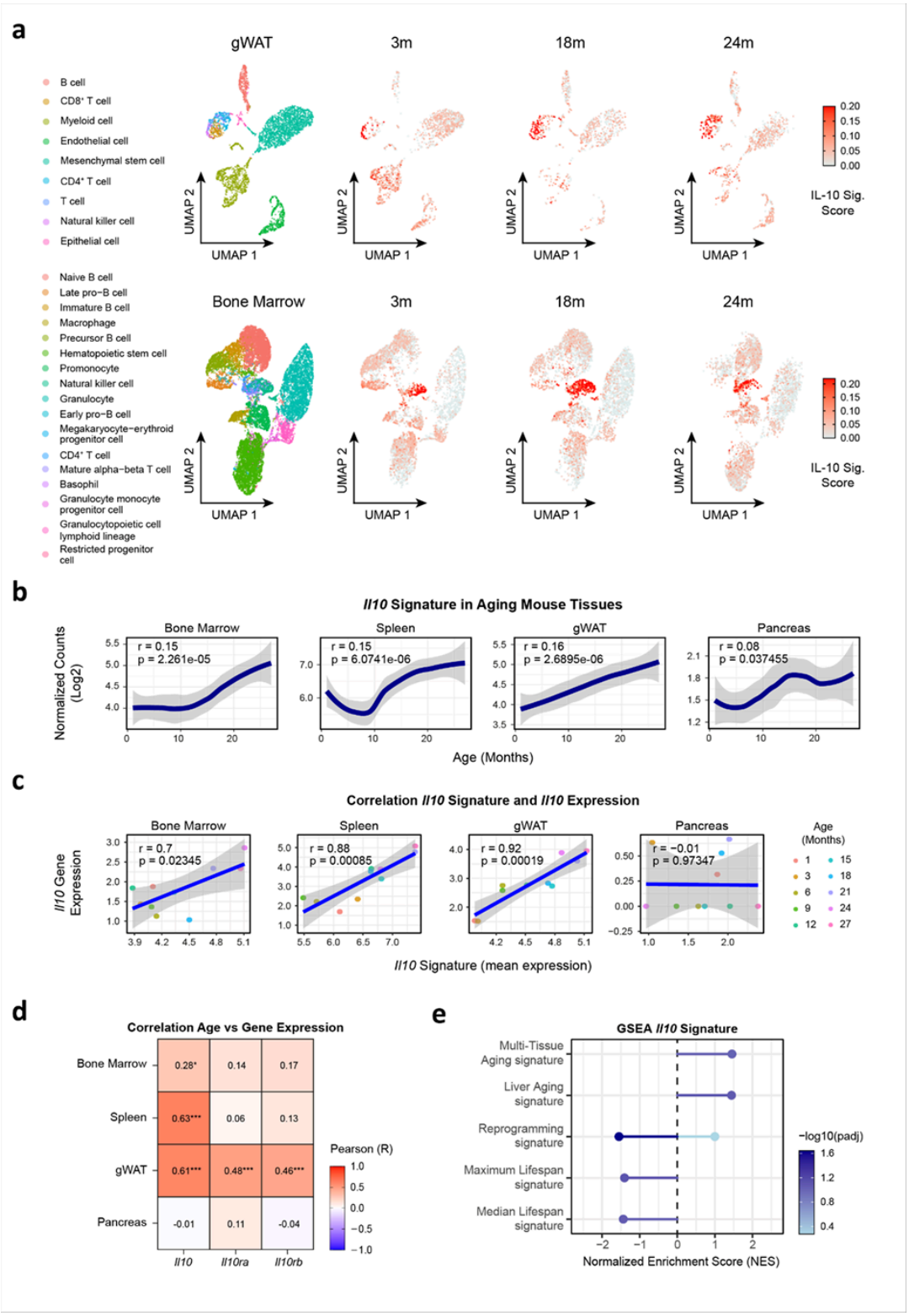


Figure 4

Dynamics of *Il10* gene expression and IL-10-induced T cell-derived signature across aging tissues. (**a**) UMAP showing the IL-10-derived T cell signature scores in individual cells of the indicated populations detected in the bone marrow and gonadal white adipose tissue (gWAT) of 3, 18 or 24 months-old mice. Data were extracted from a publicly available single-cell RNA-seq dataset [40]. (**b**) Temporal, tissue-specific trajectories of the IL-10-induced signature expression across multiple time points of the mouse life span,

for the indicated tissues. (**c**) Pearson correlation plots illustrating the relationship between the expression of *Il10* and *Il10* signature across the indicated tissues and the mouse life span indicated in months. In b and c, Pearson correlation values (*r*) and corresponding *p* values are indicated for each tissue. (**d**) Pearson correlation between the expression of the *Il10*, *Il10ra* and *Il10rb* genes and the mouse age across the indicated tissues. Statistically significant correlations are indicated: * p<0.05; *** p< 0.001. Data were extracted from the *Tabula Muris Senis* dataset of 17 different aging tissues [51]. (**e**) GSEA of the *Il10* signature in transcriptomic profiles associated with aging and lifespan-extending interventions (see Methods). Normalized enrichment scores (NES) reflect the direction and magnitude of *Il10* signature enrichment across each condition.

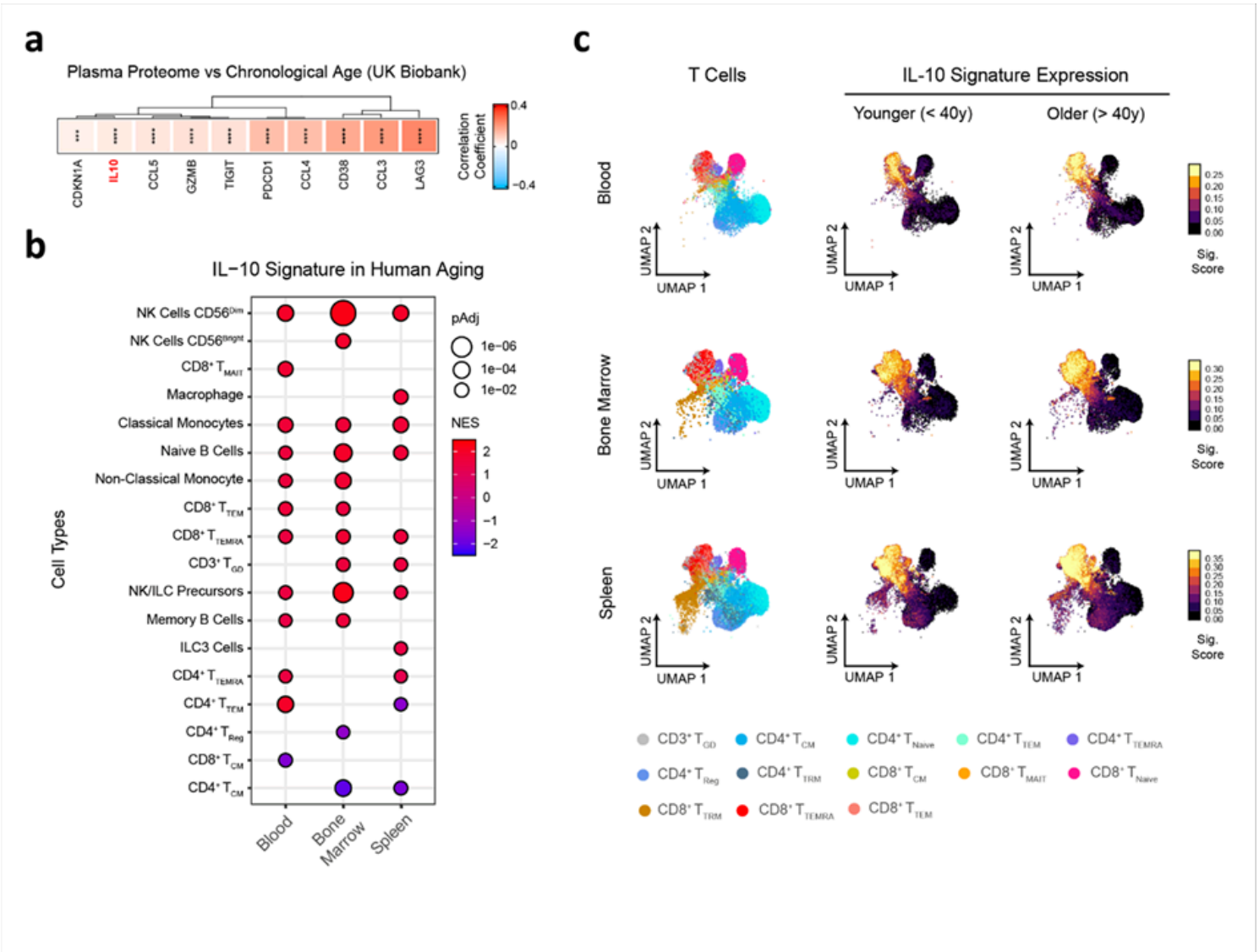


Figure 5

Dynamics of IL-10 and IL-10-induced T cell-derived transcriptional signatures in human plasma and immune cell types during aging. (**a**) Heatmap showing associations of human plasma proteins with chronological age. Human protein homologues derived from the mouse IL-10-induced transcriptional signature are shown. Results were obtained using previously processed data from the UK Biobank [45]. (**b**) GSEA analysis of the IL-10-induced transcriptional signature enriched in immune cell types across the

indicated human tissues during aging. Analyses were performed for immune cell types in the blood, spleen and bone marrow comparing over 40-years-old with under 40-years-old donors, using publicly available scRNA-seq data [46]. (**c**) UMAP plots of the IL-10-induced transcriptional signature expression in human T cells derived from the blood, bone marrow and spleen of young and aged donors. Gene expression scores were obtained using the UCell package. Statistics for plasma proteome (a) were performed by Goeminne et al [45] (***$p < 0.001$, ****$p < 0.0001$) and for sequencing data (b) are described in Methods. T_{GD}, gamma-delta T cells; T_{CM}, central memory T cells; T_{TEM}, effector memory T cells; T_{TEMRA}, effector memory re-expressing CD45RA T cells; T_{REG}, regulatory T cells; T_{TRM}, tissue-resident memory T cells; T_{MAIT}, mucosal-associated invariant T cells.

Supplementary Files

This is a list of supplementary files associated with this preprint. Click to download.

- MartinsSantosFariaSupplementarymaterial.pdf
- SupplementaryFigureLegends.docx